Zone folding and subband dispersions in GaAs-$Al_xGa_{1-x}As$(001) superlattices

M. A. Gell*
Department of Theoretical Physics, The University of Newcastle Upon Tyne, Newcastle Upon Tyne NE1 7RU, Tyne and Wear, United Kingdom

D. C. Herbert
Royal Signals and Radar Establishment, Saint Andrews Road, Great Malvern, Hereford and Worcester WR14 3PS, United Kingdom
(Received 9 December 1986)

We have used empirical pseudopotentials to show the form of the subband dispersions associated with superlattice conduction states derived from the principal and the secondary minima in several GaAs-$Al_xGa_{1-x}As$(001) superlattices. In particular, dispersions of interacting zone-center- and zone-edge-related states are shown and the zone-folding effect is demonstrated. We show that the zone-center—zone-edge mixing manifests itself in an intricate weaving of zone-center charge-density components through the charge densities of the zone-edge-related states. Along the superlattice axis, the zone-center charge density twists between each peak in the charge-density "envelopes" of the zone-edge-related states. This twisting is linked to the atomic layout within each layer and is the mechanism by which (mixed) zone-center- and zone-edge-related states are orthogonalized. Detailed comparison between results of the pseudopotential calculations and corresponding results obtained using Kronig-Penney-type analyses is made and a simple prescription is given in order to give a guide to the use of the simple model. The results suggest that in many cases the modified effective-mass Hamiltonian may be adequate for modeling hot-electron transport in superlattices, even in those consisting of ultrathin layers. We have made a thorough investigation of the role of the "camel's-back" structure at the bulk zone edges and have shown where the modified effective-mass procedures break down for zone-edge-related superlattice states.

INTRODUCTION

It has recently been shown that strong zone-folding is present in GaAs-AlAs(001) superlattices consisting of ultrathin (≤ 20 Å) layers.[1] The zone-folding effect arises as a result of mixing between bulk zone-center and bulk zone-edge Bloch components in the wave functions of the superlattice states. Optical transitions from states derived from the center of the bulk Brillouin zone (BBZ) to states derived from the edges of the BBZ, normally regarded as being forbidden, become allowed. In addition to changes in optical properties, modifications in subband dispersions also arise owing to hybridization between subbands of different curvature (effective mass). By making appropriate choices of superlattice parameters such as layer widths and aluminum fraction x (in $Al_xGa_{1-x}As$), it is possible to manipulate both optical properties and subband dispersions through the exploitation of zone-center—zone-edge mixing.

There is at present considerable interest in exploiting both optical properties and vertical transport through heterojunction multilayers for device applications. The novel band-structure effects predicted by pseudopotential calculations[1] look particularly interesting for hot-electron devices but the relevant hot-carrier transport theory is very complicated, particularly when dissipative scattering and space-charge effects are allowed for. For this reason, a simple effective-mass description of the superlattice band structure is essential to rapid progress, and a major objective of this paper is to establish the required models. With this in mind, we have studied the band structure of several GaAs-$Al_xGa_{1-x}As$(001) superlattices consisting of both thin and ultrathin layers using our pseudopotential scheme[1,2] and have, where appropriate, made direct comparison between the results of the pseudopotential calculations and corresponding results obtained using Kronig-Penney-type (KP) analyses. The parameters which are used in the effective-mass model have been taken directly from the bulk band structures within the pseudopotential calculations so that the test of the simple model is independent of errors which may be present in the pseudopotential band structures. We provide a wide-ranging guide to the use of effective-mass procedures in situations in which such models have not ordinarily been used or thoroughly tested or may not be expected to work at all. In particular, the layer widths which have been chosen allow a clear and complete picture to be presented of the role of camel's-back structures.

METHOD OF CALCULATION

In our pseudopotential method, a perturbation V is added to the Hamiltonian of a perfect infinite crystal, which in the present calculations in GaAs. The perturbation V is used to describe the changes in pseudopotential when pseudoatoms in GaAs are substituted by different species in order to form the superlattice. The superlattice wave function ψ is constructed as a unique linear combination of host-crystal Bloch functions and an eigenvalue equation is solved in order to obtain the energies of the super-

lattice states and the coefficients in each expansion of ψ. Eigenstates away from the center of the superlattice Brillouin zone (SBZ) are generated by the $\mathbf{k}\cdot\mathbf{p}$ method. The technical details of this pseudopotential method can be found elsewhere.[1,3] For the purposes of the present work, we show in Table I values of various quantities from our pseudopotential calculations which may be useful in a scheme based on parametrization.[5] The local pseudopotential form factors used in the calculations are given elsewhere.[1] Coefficients c_n of fifth-order minimax polynomials fitted to the lowest conduction band of GaAs and AlAs along the Δ line for $0.65(2\pi/a) \leq k_z \leq 1.0(2\pi/a)$ are also shown in Table I; a is the lattice constant, taken to be the same in GaAs and AlAs. The bulk zone-edge levels $E_{\mathrm{BBZ}}(k_z)$ in eV are given by

$$E_{\mathrm{BBZ}}(k_z)=\sum_{n=0}^{5} C_n k_z^n , \tag{1}$$

where k_z is in units of $2\pi/a$. These results may be compared for example with the results presented by Kopylov.[4] It should be noted that the parameters which are given for AlAs correspond to the band structure which is calculated within the superlattice pseudopotential scheme by changing all monolayers of GaAs into AlAs. The AlAs parameters, owing to convergence problems associated with expanding AlAs Bloch functions in terms of a limited basis set of GaAs Bloch functions, are slightly different from those which would be obtained directly from the AlAs form factors.[3] However, since one of the objectives of this work is to make a direct comparison between pseudopotential and effective-mass results, the parameters which are used for AlAs correspond to the band structure which is "seen" in the superlattice calculation. By keeping the energies of the Γ_6^c and X_6^c levels of GaAs fixed, the corresponding energies for the Γ_6^c and X_6^c levels of $Al_xGa_{1-x}As$ can be found by linear interpolation between the values given in Table I. The agreement between the values obtained by such linear interpolation and the values obtained from the pseudopotential calculations, in which the virtual crystal approximation is used to model the alloy, is within 1 meV.

In order to calculate superlattice states within the framework of a Kronig-Penney-type model, we adopt the approach described by Vigneron and Lambin.[6,7] Their approach is particularly suited to extensions of the basic Kronig-Penney model in which, for example, potentials of arbitrary shape and dimension, electric fields, and energy-dependent masses can be included. This is an important consideration for the purposes of device modeling.

In order to describe the lowest zone-center-related conduction states EΓn and EΓRn ($n=1,2,\ldots$ with $n=1$ corresponding to the state of lowest energy; R is used to denote a resonant state) in the Kronig-Penney–type models, we have used several prescriptions for the effective mass. One approach uses an average zone-center effective mass $\overline{m}^*_\Gamma$ defined by

$$\overline{m}^*_\Gamma = m^*_{A,\Gamma} + \frac{xL_B(m^*_{B,\Gamma}-m^*_{A,\Gamma})}{L_A+L_B} , \tag{2}$$

where x is the aluminum fraction in the alloy layer of width L_B with effective mass $m^*_{B,\Gamma}$, and $m^*_{A,\Gamma}$ is the effective mass in the GaAs layer of width L_A. The values of $m^*_{A,\Gamma}$ and $m^*_{B,\Gamma}$ have been given in Table I. In order to take account of nonparabolicity in the zone-center region of the lowest conduction band of GaAs, we use the expression

$$m^*_{A,\Gamma}(E)=m^*_{A,\Gamma}(1+\alpha^\Gamma E) , \tag{3}$$

where E is energy.[8] The value of the constant α has been given in Table I. The prescriptions for the effective

TABLE I. Table showing various quantities in the pseudopotential calculations which are used as input to the Kronig-Penney–type analyses to provide a realistic test of effective-mass modeling. See the text for further comments. The figures in parentheses are those given by Kopylov (Ref. 4).

	GaAs	AlAs
Γ_6^c level	1.523 eV	2.473 eV
X_6^c level	2.012 eV	1.738 eV
Depth of Δ_5 minimum	14.5 meV (9.3 meV)	10.4 meV (0.2 meV)
Wave vector along the Δ line from the X point to the bottom of the Δ_5 minimum, κ (in units of $2\pi/a$)	0.10 (0.102)	0.08 (0.042)
Polynomial coefficients c_n		
$n=0$	15.5766	13.3380
$n=1$	−75.8805	−61.7111
$n=2$	189.232	149.482
$n=3$	−251.589	−195.999
$n=4$	171.098	132.232
$n=5$	−46.4255	−35.6043
Effective mass at Γ_6^c	$m^*_{A,\Gamma}=0.077m_0$	$m^*_{B,\Gamma}=0.143m_0$
Nonparabolicity factor, α^Γ	0.559 eV^{-1}	
Nonparabolicity factor, α^X	−0.588 eV^{-1}	−0.516 eV^{-1}
Lattice constant, a	5.654 Å	5.654 Å

TABLE II. Table giving the prescriptions for the effective masses used in the Kronig-Penney–type (KP) analyses for the zone-center- and zone-edge-related states. The label $(+np)$ is used to denote "with nonparabolicity" and the label $(-np)$ is used to denote "without nonparabolicity." Label A is used for GaAs and label B is used for $Al_xGa_{1-x}As$.

Prescription	Zone-center-related states	Zone-edge-related states
KP$(-np)$	Average effective mass as given by Eq. (2) using $m^*_{A,\Gamma}$ and $m^*_{B,\Gamma}$	
KP$(+np)$	Average effective mass as given by Eq. (2) using $m^*_{A,\Gamma}(E)$ and $m^*_{B,\Gamma}$	
KP1$(-np)$	Different effective mass $(m^*_{A,\Gamma}, m^*_{B,\Gamma})$ in each layer	
KP1$(+np)$	Different effective mass $[m^*_{A,\Gamma}(E), m^*_{B,\Gamma}]$ in each layer	
KP		Average effective mass as given by Eq. (9)
KP1		Different effective mass $(m^{**}_{A,X}, m^{**}_{B,X})$ in each layer
KP2		$m^{**}_{B,X}$ used in both layers

masses which are used in the various calculations are given in Table II. Discontinuities in the potential V and in the effective masses are handled by setting V and $2m^*(V-E)$ to their mean values at the interface.[6,7]

In the region of the zone edge, the lowest conduction band may be approximated by

$$E(k)=\frac{\hbar^2}{2m^*_X}(k-\kappa)^2 , \tag{4}$$

where κ, given in Table I, is the wave vector from the X point to the bottom of the Δ_5 minimum and wave vector k is measured from the X point. The effective mass m^*_X is obtained by fitting the band structure for $k>\kappa$ to the form

$$\frac{\hbar^2k^2}{2m_X}=E(1+\alpha^X E) \tag{5}$$

and writing

$$m^*_X=m_X(1+\alpha^X E) . \tag{6}$$

For GaAs (labeled A), we find $m_{A,X}=1.35m_0$ and $\alpha^X_A=-0.588$ eV^{-1} and for AlAs (labeled B), we find $m_{B,X}=1.40m_0$ and $\alpha^X_B=-0.516$ eV^{-1}. These values were obtained by fitting to points approximately 6 and 350 meV above the bottom of the Δ_5 minimum in the region with $k>\kappa$. Within the Vigneron-Lambin method, we include the camel's-back structure through an energy-dependent effective mass, m^{**}_X. We equate

$$\frac{\hbar^2}{2m^*_X}(k-\kappa)^2=\frac{\hbar^2}{2m^{**}_X}k^2 \tag{7}$$

which gives

$$m^{**}_X=\frac{2m^*_XE+\kappa^2\pm2\kappa(2m^*_XE)^{1/2}}{2E} , \tag{8}$$

where the positive root is taken for $k>\kappa$. Within the barrier (GaAs) region, we obtain m^{**}_X from Eq. (8) if $|V-E|>14.5$ meV but set $m^{**}_X=m_{A,X}$ (constant) if $|V-E|\leq 14.5$ meV. In order to define an average effective mass, we use

$$\overline{m}^{**}_X=\frac{l_Am^{**}_{A,X}+L_Bm^{**}_{B,X}(x)}{l_A+L_B} , \tag{9}$$

where the length $l_A\leq L_A$ is taken to be either the tunneling length given by

$$l=2(2m^{**}_{A,X}|V-E|)^{-1/2} \tag{10}$$

or the length L_A of the barrier region depending which has the smallest value. This approach has been adopted owing to the small decay lengths which are usually associated with the zone-edge-related conduction states. The prescriptions for the effective masses which are used in the calculations are given in Table II.

RESULTS AND DISCUSSIONS

We consider first the accuracy and reliability of our pseudopotential calculations. Within our pseudopotential method in its present form, the symmetric and antisymmetric form factors of GaAs and AlAs at the bulk reciprocal-lattice vectors are fixed. However, interpolation of the potential between these Fourier components is somewhat arbitrary. Since we use a virtual-crystal approximation in order to achieve a rigid shift of one bulk band structure with respect to the other, the value of the symmetric Fourier component of the superlattice local potential $V^S_L(q)$ at wave vector $q=0$ is also fixed. We neglect effects such as reconstruction at the interfaces. At $q=0$, the structure factor eliminates the antisymmetric component of the superlattice local potential $V^A_L(q)$ and so $V^A_L(0)$ does not affect band offsets. The value of $V^A_L(0)$, unlike that of $V^S_L(0)$, is therefore somewhat arbitrary. Insight into the reliability of the pseudopotential calculations can be obtained by testing the effects on energy levels (and optical matrix elements) of various changes to the

superlattice potential. For example, keeping $V_L^S(0)$ (i.e., the band offset) constant, changes can be made to the potential, especially in the small-q region, by shifting $V_L^A(0)$ and fitting new antisymmetric potential curves (e.g., by Lagrange interpolation) between the fixed antisymmetric bulk form factors. In order to focus on a rather difficult test of the potential, we shall consider a superlattice, the GaAs(5.7 Å)/AlAs(5.7 Å) (001) superlattice with 60:40 offsets, for which extensive results, obtained using $V_L^A(0)=0$, have already been presented.[1]

At the center of the SBZ in the GaAs(5.7 Å)/AlAs(5.7 Å) superlattice, the states lying closest to the forbidden gap are (in the notation of Ref. 1) the ground split-off (V3), the ground light-hole-like state (V2), the ground heavy-hole-like state (V1), and the three lowest conduction-band states (C1, C2, and C3). States C1, C2, and C3 are states derived from both the center and edges of the BBZ. Energy-wave-vector dispersion curves for these states have been presented in Ref. 1. Here, we focus on the stability of the energy levels with respect to large changes in the superlattice potential. By setting the values of $V_L^A(0)$ to ± 0.011 atomic units normalized to unit volume, additional curves are obtained for the superlattice antisymmetric potential. Thus, three separate calculations (with $V_L^A(0)=0$, ± 0.011 normalized a.u.) can be performed in which the bulk band structures and the band offsets are kept the same, but scattering processes, especially at long wavelength, are very different. In Table III, we show the differences between the energy levels for the six states at the center of the SBZ for the two additional calculations compared with the results already given in Ref. 1 for the case of $V_L^A(0)=0$. Bearing in mind the large changes which have been made to the superlattice

TABLE III. Table showing the change in energy in meV of the states at the center of the superlattice Brillouin zone in the GaAs(5.7 Å)/AlAs(5.7 Å) (001) superlattice with the change in the superlattice antisymmetric local pseudopotential $V_L^A(q)$ in atomic units normalized to unit volume, defined by the component at $q=0$. Energy-wave-vector dispersion curves of the states, calculated with 60:40 offsets and with $V_L^A(0)=0$, have been given in Ref. 1. The labeling of the states is explained in the text and is the same as that used in Ref. 1.

	$V_L^A(0)$	
Superlattice state	-0.011 (normalized a.u.)	$+0.011$ (normalized a.u.)
C3	2	−5
C2	−5	8
C1	−18	11
V1	−4	6
V2	−2	3
V3	−3	4

TABLE IV. Table showing energies (in meV), subband widths (in meV), and the SBZ-center effective mass (in units of free-electron mass) of the lowest zone-center-related conduction state EΓ1 and the energy at the edge of the SBZ of state EΓR1 in the GaAs(11.3 Å)/$Al_xGa_{1-x}As$(45.2 Å) (001) superlattice. The results have been obtained using the pseudopotential method (PP) and Kronig-Penney–type (KP) models with various prescriptions (see Table II) for the effective mass. Owing to intricate mixings between states for high values of x, some values of energy have been omitted.

Aluminum fraction	Method	EΓ1 energy at Γ_{SBZ} (meV)	EΓ1 energy at X_{SBZ} (meV)	EΓ1 subband width (meV)	EΓ1 effective mass at Γ_{SBZ} (m_0)	EΓR1 energy at X_{SBZ} (meV)
0.2	PP	147	244	97	0.092	310
	KP($+np$)	147	237	90	0.085	310
	KP($-np$)	147	250	103	0.076	326
	KP1($+np$)	152	256	104	0.086	308
	KP1($-np$)	153	262	109	0.079	322
0.3	PP	214	289	75	0.104	394
	KP($+np$)	214	282	68	0.099	396
	KP($-np$)	215	295	80	0.088	412
	KP1($+np$)	224	298	74	0.096	394
	KP1($-np$)	228	318	90	0.087	408
0.4	PP	276	330	54	0.127	
	KP($+np$)	275	325	50	0.118	483
	KP($-np$)	278	338	60	0.106	499
	KP1($+np$)	293	349	56	0.112	481
	KP1($-np$)	302	375	73	0.097	494
0.5	PP	321	339	18	0.255	
	KP($+np$)	330	365	35	0.152	571
	KP($-np$)	334	378	44	0.123	586
	KP1($+np$)	358	400	42	0.138	569
	KP1($-np$)	374	433	59	0.108	582

potential, it is clear from Table III that uncertainties in the superlattice energy levels due to "uncertainties" in the superlattice potential are no more than a few meV. The largest variations in energy level are always seen in those superlattice states dominated by strong Γ-X mixing. Since the GaAs(5.7 Å)/AlAs(5.7 Å) superlattice provides a rather extreme test of the superlattice potential (the layers each consist only of two monolayers), we suggest that the uncertainties illustrated in Table III represent rather extreme limits. Extensive tests and discussions on the role of the superlattice potential, in terms both of energy levels and optical matrix elements, in systems consisting of thicker (20—100 Å) layers have been presented elsewhere.[3,9,10] For cases in which strong zone-center—zone-edge mixing is not present, we suggest that uncertainties in the energy levels of the conduction states are generally no more than about 2—5 meV.

The parameters in the pseudopotential models are adjusted to fit experimental values for band gaps of bulk crystals (GaAs and AlAs). The resulting masses, however, deviate slightly from experimental values but can be adjusted within a $\mathbf{k}\cdot\mathbf{p}$ approach. To provide a stringent test of effective-mass models, masses for GaAs and AlAs are taken *directly* from the pseudopotential band structures. If the resulting effective-mass models agree well with the pseudopotential band structures of superlattices, then it may be expected that the effective-mass models when used with experimental values for masses and offsets should provide a good description of electronic structure for device modeling purposes.

GaAs(11.3 Å)/$Al_xGa_{1-x}As$(45.2 Å) (001) SUPERLATTICE

In Fig. 1, we show the dispersions along the Δ_z line of the SBZ of the lowest zone-center-related conduction state EΓ1 in the GaAs(11.3 Å)/$Al_xGa_{1-x}As$(45.2 Å) superlattice for $x=0.2$, 0.3, 0.4, and 0.5. The dashed lines show the variation with aluminum fraction x of the Γ_6^c and X_6^c levels of the alloy. It should be noted that the signs of the effective potential wells (EPW's) associated with the bulk zone center and bulk zone edge are opposite, corresponding here to the situation obtained with a band alignment between GaAs and AlAs in which 60% of the difference in band gaps at the center of the BBZ is taken up as the discontinuity between the two Γ_6^c levels. Zone-center-related bound states are confined (apart from leakage) in the GaAs layers, whilst zone-edge-related bound states are confined in the alloy layers. The resonant states, both zone-center- and zone-edge-related, are confined in those layers in which the corresponding bound states are not confined. The decreasing subband width of EΓ1 with increasing aluminum fraction arises from the increasing height of the Γ_6^c EPW.

In Table IV, we compare the energies, subband width, and the SBZ-center effective mass of EΓ1 obtained using the pseudopotential (PP) method and Kronig-Penney—type (KP) models with various prescriptions for the effective masses (see Table II). It can be seen from Table IV that the best agreement between the PP and KP results for $x<0.5$ is obtained using an *averaged* effective mass in the simple model rather than a *different* mass in each region. In order to shed light on the large discrepancies for $x=0.5$, we show in Fig. 2 for $x=0.4$ and in Fig. 3 for $x=0.5$, the dispersions of the lowest conduction states up to the highest-excited zone-edge-related bound state EX4. We denote the zone-edge-related bound states by E$X$$n$ with integer n increasing from 1 with increasing energy. The dispersions in Fig. 2 demonstrate the small subband widths (large effective masses) which are associated with the zone-edge-related states. For cases in which the barrier (GaAs) to these states is much bigger ($\gtrsim$40 Å) than the barrier (11.3 Å) considered here, there is little tunneling (in the absence of zone-center—zone-edge mixing) and the subband widths of the zone-edge-related states may be less than 1 meV[2]. The dispersions shown in Fig. 3 show significant departure from the behavior shown in Fig. 2. For example, state EX2 in Fig. 3, lying in a deeper zone-edge EPW than state EX2 in Fig. 2, has significant dispersion. The increase in dispersion has arisen as a result of mixing zone-center components from state EΓ1 into the wave function of state EX2. Conversely, zone-edge components are mixed into the wave function of state EΓ1 and its dispersion is reduced compared with what it would have been if no zone-center—zone-edge

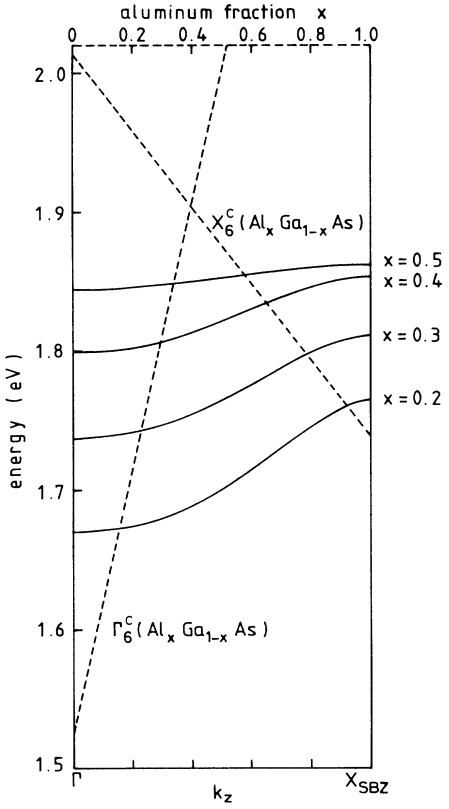

FIG. 1. Dispersions along the Δ_z line (bottom scale) between Γ_{SBZ} and X_{SBZ} of the lowest zone-center-related conduction state EΓ1 in the GaAs(11.3 Å)/$Al_xGa_{1-x}As$(45.2 Å) (001) superlattices with $x=0.2$, 0.3, 0.4, and 0.5. The dashed lines show the variation with aluminum fraction x (top scale) of the Γ_6^c and X_6^c levels of the alloy.

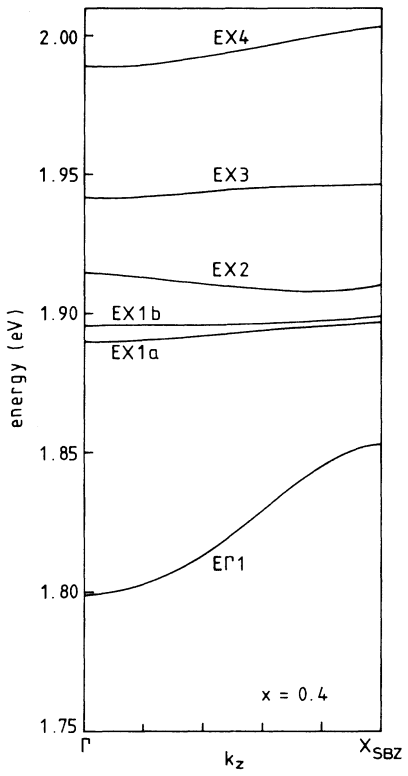

FIG. 2. Dispersions along the Δ_z line between Γ_{SBZ} and X_{SBZ} of the lowest conduction states in the GaAS(11.3 Å)/$Al_{0.4}Ga_{0.6}As$(45.2 Å) (001) superlattice. The dispersion of state EΓ1 has already been given in Fig. 1. Note that the zone-edge-related states EXn have very little dispersion compared with the zone-center-related state EΓ1. The ground zone-edge related state EX1 comprises a pair of quasidegenerate states arising from the two equivalent Δ_5 minima lying approximately $(0,0,0.08)2\pi/a$ in from the edges ($\pm X$) of the $Al_xGa_{1-x}As$ BBZ.

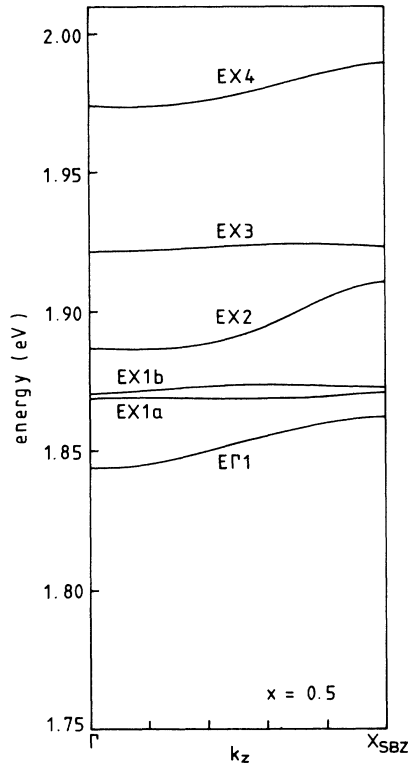

FIG. 3. Dispersions along the Δ_z line between Γ_{SBZ} and X_{SBZ} of the lowest conduction states in the GaAs(11.3 Å)/$Al_{0.5}Ga_{0.5}As$(45.2 Å) (001) superlattice. The dispersion of state EΓ1 has already been given in Fig. 1. Interaction has taken place between state EΓ1 and, in particular, state EX2 and has led to significant changes in the dispersion curves compared with those shown for the EXn in Fig. 2.

mixing had taken place. The discrepancy between the pseudopotential and Kronig-Penney—type results in Table IV for $x=0.5$ can now be understood.

It can be seen from Fig. 2, that two states (E$X1a$ and E$X1b$) have been indicated as being the ground zone-edge-related bound state. This double quasidegeneracy (DQD) is due to the fact that in the lowest conduction band of $Al_xGa_{1-x}As$ (and GaAs), the secondary minima on the Δ line between $(0,0,-1)2\pi/a$ and $(0,0,1)2\pi/a$ do not lie exactly at the edges ($\pm X$) of the BBZ. The two equivalent Δ_5 minima, calculated to be 14.5-meV deep in GaAs (see Table I), may give rise to a pair of states trapped inside the Δ_5 minima. The existence of such a DQD and the number of states depends on the thickness of the layer and the width in wave-vector space of the Δ_5 minima.

For those cases in which one DQD has arisen (as here), the total wave function Ψ of the DQD is formed from a linear combination of the even wave functions ψ_s from each of the two equivalent Δ_5 minima. Orthogonality of the zone-edge-related bound states directly above the X_6^c point to those states trapped inside the Δ_5 minima is achieved by the different rapidly varying Bloch components which make up the superlattice states. This contrasts, for example, with the descriptions based on the envelope-function approximation in which orthogonality of the zone-center-related bound states is controlled by envelope functions and information about the rapidly varying Bloch components is largely ignored. It can be seen from Fig. 3 that state EΓ1 anticrosses (mixes with) state EX2; state EΓ1 also anticrosses state EX4 but crosses (or, rather, mixes very weakly with) state EX3. It appears to be a general rule from all GaAs-$Al_xGa_{1-x}As$ superlattices which we have studied that state EΓ1 anticrosses the zone-edge-related state immediately above those states with DQD trapped in the $Al_xGa_{1-x}As$ Δ_5 minima.[3] This rule gives a prescription for predicting (anti)crossings between the other conduction states. In Table V, we show the subband energies for the zone-edge-related states using the pseudopotential method and Kronig-Penney—type models. The results obtained using the prescription KP2 (see Table II) correspond to the case in which the alloy ef-

TABLE V. Energies in meV calculated for the zone-edge-related states in the GaAs(11.3 Å)/$Al_{0.4}Ga_{0.6}As$(45.2 Å) (001) superlattice using the pseudopotential (PP) method and Kronig-Penney–type (KP) models (see Table II). The results indicated with an asterisk have been obtained using an infinite-square-well model combined with the pseudopotential band structure. The (+) and (−) indicate results obtained using the positive and negative roots in Eq. (8).

	Superlattice state				
Method	E$X1a$	E$X1b$	E$X2$	E$X3$	E$X4$
PP	2–9	8–11	21–26	54–59	101–115
KP	4.3 (+)	4.9 (−)	23–23.5	54–57	83–88
KP1	1–1.3(−)	4.6–4.9(+)	18–19.5	55.6–60	102–115
KP2	2–2(*)	2.8–2.8(*)	21–21	55–59	99–117

fective mass $m^{**}_{B,X}$ is used in both the alloy and the GaAs layers; such a prescription may be appropriate because the GaAs layer is only 11.3 Å in thickness. Approximate energies for states E$X1a$ and E$X1b$ may be obtained using an infinite square-well model combined with the pseudopotential band structure. Defining wave vectors $k_n = n\pi/L_B$ ($n=1,2,\ldots$), energies of 2.8 meV ($n=1$) and 2.0 meV ($n=2$) may be calculated from the polynomials whose coefficients are given in Table I.

The charge densities shown in Fig. 4 of state E$X2$ at the center and the edge of the SBZ in the superlattice with $x=0.4$ and $x=0.5$ indicate the disruption caused by the interaction with state E$\Gamma 1$. This disruption is especially evident at the edge of the SBZ as might be expected from the dispersion curves shown in Figs. 2 and 3. Since only limited information can be given by a charge-density plot along a line in the [001] direction, we show in Fig. 5(a) a charge-density contour plot of state E$X2$ at the edge of the SBZ for $x=0.4$. The charge density has been plotted over an area spanning five lattice constants by five lattice constants in an xz plane which passes through anion (As) sites. The positions of the anions have been indicated by solid circles. The GaAs layer is shown completely although only $\frac{3}{8}$ of the $Al_xGa_{1-x}As$ layer has been shown; this will not, however, restrict our study. In Fig. 5(b), we show the corresponding charge density of state E$X2$ remaining after all zone-center charge-density components have been removed by artificially setting to zero the appropriate coefficients in the expansion of ψ. For the purposes of this charge-density plot, we have defined the zone-center region to be that part of the Δ line in the BBZ lying between $\mathbf{k}=(0,0,-0.5)2\pi/a$ and $k=(0,0,0.5)2\pi/a$. It can be seen from Fig. 5(b) that the underlying charge density of state E$X2$ is rather like the delocalized charge density associated with zone-edge states in bulk III-V materials;[11,12] almost all of the charge sits in the interstitial regions between the nuclei. Apart from the alternating protrusions of charge at the GaAs-$Al_xGa_{1-x}As$ interfaces, there is no zone-edge charge density in the GaAs layer. However, the contour plot of the *full* charge density of state E$X2$ in Fig. 5(a) shows significant charge in the GaAs region. This charge is related to the zone-center components which have been introduced into the wave function of state E$X2$ due to its interaction with state E$\Gamma 1$ and is distinct from the zone-edge charge since it sits mostly on the anion (and cation) sites. The spatial localization of the zone-center charge-density components is similar to that found at the zone-center Γ^c_6 of bulk III-V materials. However, the zone-center charge-density components in E$X2$ on the left-hand side (LHS) GaAs-$Al_xGa_{1-x}As$ interface reside, along the [100] direction, in alternate pairs of anions. On the right-hand side interface (right edge of picture), these charge-density components also reside in alternate pairs of anions but are staggered with respect to those at the LHS interface.

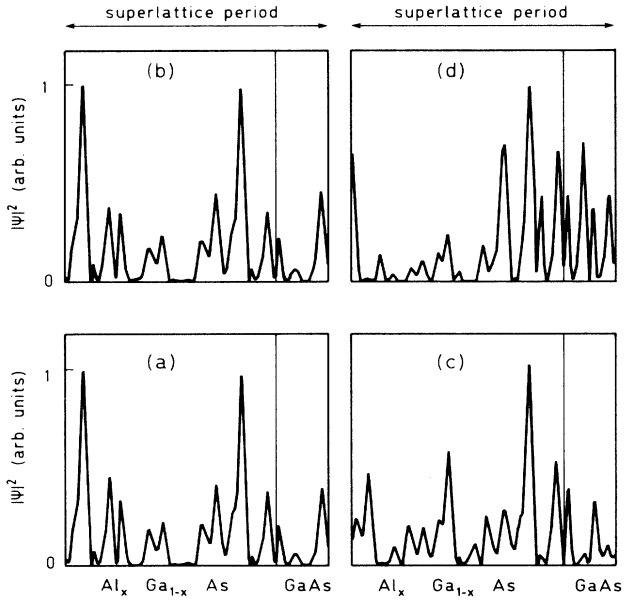

FIG. 4. Left-hand side: Charge density of state E$X2$, plotted along the superlattice axis in the [001] direction, at the *center* of the SBZ in the GaAs(11.3 Å)/$Al_xGa_{1-x}As$(45.2 Å) (001) superlattice for (a) $x=0.4$ and (b) $x=0.5$. The charge densities have been plotted along a line which passes through mid-bond positions and the peak of $|\psi|^2$ has been set to 1 to facilitate presentation. Right-hand side: Charge density of state E$X2$, plotted along the superlattice axis in the [001] direction, at the *edge* of the SBZ in the GaAs(11.3 Å)/$Al_xGa_{1-x}As$(45.2 Å) (001) superlattice for (c) $x=0.4$ and (d) $x=0.5$. Zone-center-related charge-density components have been introduced into state E$X2$ owing to its interaction with state E$\Gamma 1$ (see Figs. 2 and 3). This interaction has led to a strong zone-folding effect (see Table VI).

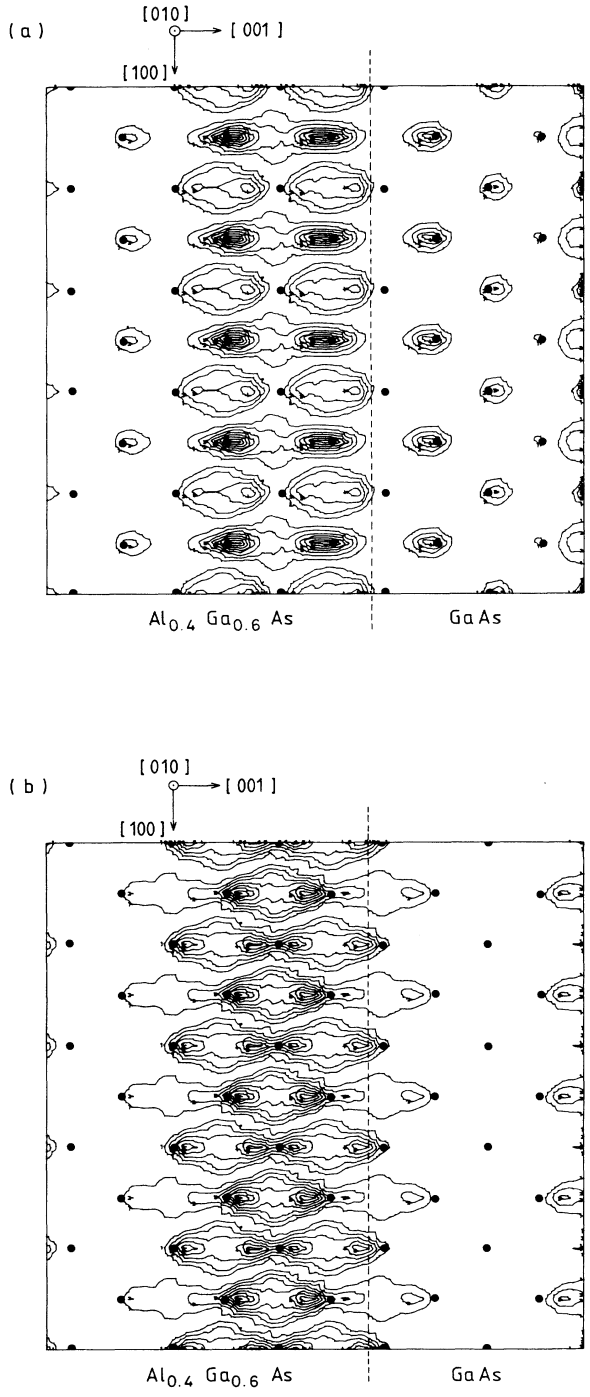

FIG. 5. (a) Charge-density contour plot of state EX2 at the edge of the superlattice Brillouin zone in the GaAs(11.3 Å)/$Al_{0.4}Ga_{0.6}As$(45.2 Å) (001) superlattice. The charge density has been plotted over an area spanning five lattice constants by five lattice constants in an xz plane which passes through anion (As) sites. The positions of the anions have been indicated by solid dots. The GaAs layer is shown completely although only $\frac{3}{8}$ of the $Al_xGa_{1-x}As$ layer has been shown. (b) Charge density from (a) remaining after the zone-center charge-density components have been removed (see the text).

In Fig. 6, we show full charge-density contour plots for (a) state EX2, (b) state EX3, and (c) state EX4 at the edge of the SBZ for the case $x=0.5$. From our earlier discussion, especially concerning the dispersions in Fig. 3, we expect the effects of zone-center–zone-edge mixing to be particularly evident in states EX2 and EX4. In fact, Fig. 6(a) shows a charge density which is dominated by zone-center components. The charge density shown in Fig. 6(c) is similar to the hybrid zone-center–zone-edge charge density shown in Fig. 5(a); these charge densities are complementary to the charge density of EΓ1 (not shown). The bands of charge density lying in the [100] direction which are shown in Fig. 6(c) correspond to two of the four peaks in the [001]-direction charge-density "envelope" of the third-excited bound state EX4. Between neighboring peaks of the envelope, the localization of the zone-center charge-density components in alternate pairs of anions (passing along the [100] direction) is staggered. The admixture of zone-center charge density into state EX4 (as well as state EX2) has occurred as an intricate weaving action through the $Al_xGa_{1-x}As$ layer. The charge-density contour plot given in Fig. 6(b) shows that little zone-center charge density is present in state EX3; the delocalized nature of the charge density is similar to that shown in Fig. 5(b).

In order to demonstrate the zone-folding effect and give further insight into the effect of zone-center–zone-edge mixing, we have calculated various modulus squared optical matrix elements $M_{if}=|\langle\psi_f|\hat{\mathbf{P}}|\psi_i\rangle|^2$ for the superlattice with $x=0.5$. The ψ_i and ψ_f refer to the initial and final state wave functions and $\hat{\mathbf{P}}$ is the momentum operator chosen to lie in either the [110] or [001] direction. Squared optical matrix elements calculated at the center and at the edge of the SBZ are shown in Table VI. Transitions corresponding to M_{if} with values less than 10^{-9} a.u. have been omitted; these transitions may be regarded as being forbidden. We consider first the transitions from the ground heavy-hole-like state HH1 to the conduction states. The M_{if} for the transitions to EΓ1 show that, even though the GaAs layer is only two lattice constants in width, the selection rule based on the polarization $\hat{\mathbf{P}}$ is obeyed both at the center and at the edge of the SBZ; since the heavy-hole-like state has no $|z\rangle$ component in its wave function, transitions with (001) polarization are forbidden. The M_{if} for the transitions to the EXn from the ground heavy-hole-like state are comparable with or at most only 3 orders of magnitude smaller than the transitions to EΓ1 and therefore correspond to transitions which have, in principle, become allowed, i.e., observable in experiment. This is the zone-folding effect. We note that in real GaAs-$Al_xGa_{1-x}As$ systems, the zone-folding effect can occur as a result of changes in alloy composition (as described here) or changes in the widths of the layers or may be induced by the application of hydrostatic pressure.[1,3,13] M_{if} for the transition HH1 to EX2 at the edge of the SBZ is especially large as might be expected from the dispersion curve in Fig. 3 and the contour plot in Fig. 6(a). We next consider transitions between the various conduction states. It can be seen from Table VI that such transitions, both at the center and edge of the SBZ, may be allowed with $\hat{\mathbf{P}}$ lying in the [001] direction. The

symmetry of the zone-edge-related states alternates between s-like (totally symmetric) and z-like with the strongest transitions occurring between the states of different symmetry.[14,15]

Optical matrix elements of similar magnitude are found for transitions between zone-center-related bound and/or resonant states in GaAs-$Al_xGa_{1-x}As$ superlattices consisting of thicker (50—100 Å) layers[16] and large-dipole infrared transitions have been observed within the conduction band of a GaAs quantum well.[17]

The transitions between zone-edge-related states may be useful for device applications since the states have little dispersion and their energy levels can be tuned by changing the alloy composition.

GaAs(28.3 Å)/$Al_xGa_{1-x}As$(28.3 Å) (001) SUPERLATTICE

In Fig. 7, we show the dispersions along the Δ_z line of the SBZ of the lowest conduction states in the GaAs(28.3

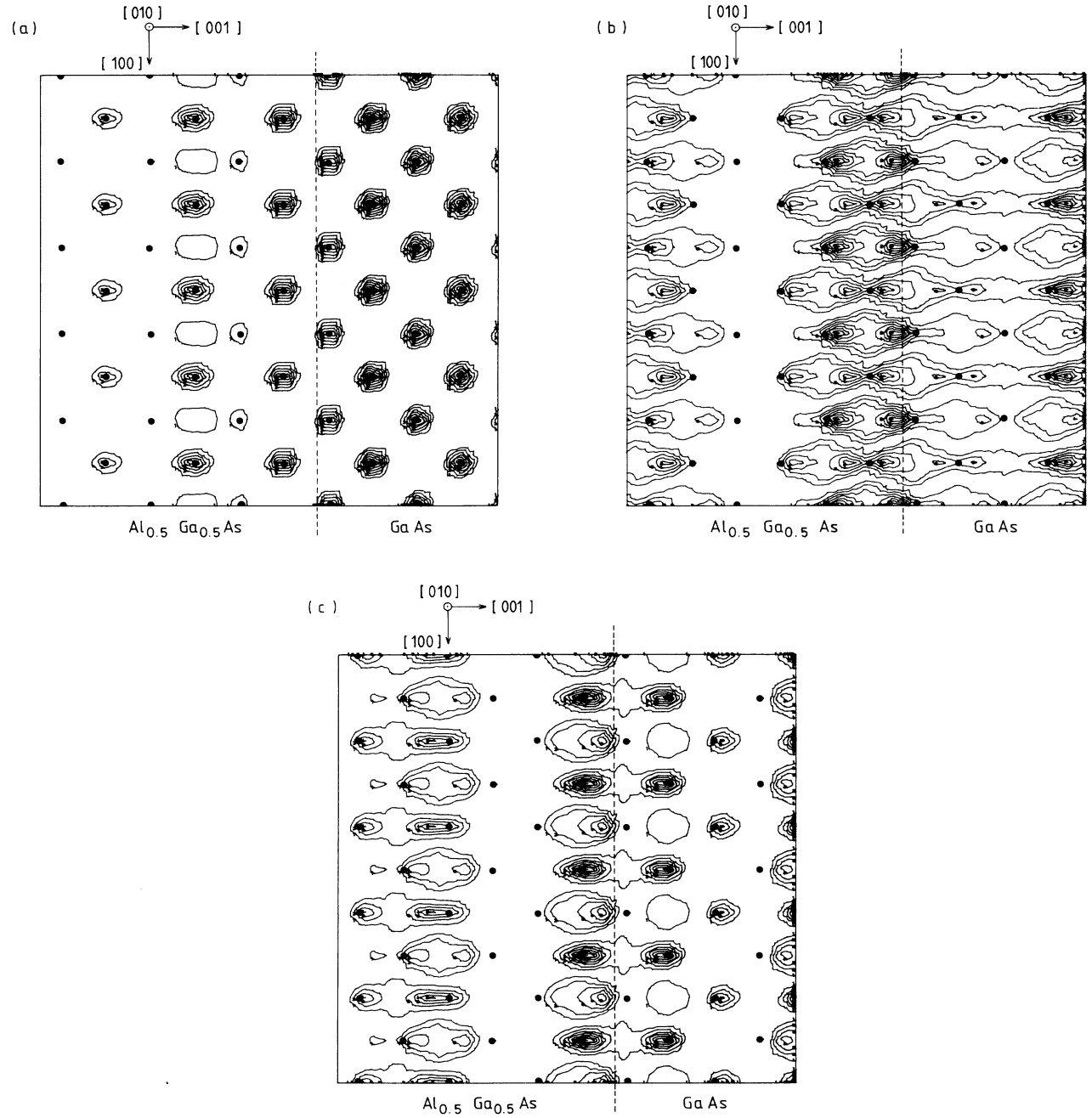

FIG. 6. Charge-density contour plot of (a) state EX2, (b) state EX3, and (c) state EX4 at the edge of the superlattice Brillouin zone in the GaAs(11.3 Å)/$Al_{0.5}Ga_{0.5}As$(45.2 Å) (001) superlattice. See the caption to Fig. 5 for further details.

TABLE VI. Table showing modulus squared optical matrix elements M_{if} in atomic units calculated with (110) and (001) polarizations for various transitions between states at the center and at the edge of the SBZ in the GaAs(11.3 Å)/$Al_{0.5}Ga_{0.5}As$(45.2 Å) (001) superlattice. The conduction states EΓ1 and EX*n* are those which have been shown in Fig. 3. The label HH1 denotes the ground heavy-hole-like bound state in the valence band. Transitions corresponding to M_{if} with values less than 10^{-9} a.u. have been omitted.

Modulus squared matrix element at the center of the SBZ (a.u.) Polarization		Modulus squared matrix element at the edge of the SBZ (a.u.) Polarization		Initial	Final
(110)	(001)	(110)	(001)	state	state
0.16		0.55×10^{-1}		HH1	EΓ1
0.14×10^{-2}		0.34×10^{-2}		HH1	EX1*a*
0.72×10^{-1}		0.16×10^{-1}		HH1	EX1*b*
0.17×10^{-2}		0.18		HH1	EX2
0.23×10^{-1}		0.34×10^{-3}		HH1	EX3
0.24×10^{-4}		0.21×10^{-1}		HH1	EX4
	0.15×10^{-5}		0.17×10^{-3}	EΓ1	EX1*a*
	0.45×10^{-6}		0.16×10^{-3}	EΓ1	EX1*b*
	0.14×10^{-3}		0.11×10^{-4}	EΓ1	EX2
	0.11×10^{-4}		0.17×10^{-4}	EΓ1	EX3
	0.59×10^{-6}		0.52×10^{-6}	EΓ1	EX4
	0.97×10^{-5}		0.89×10^{-4}	EX1*a*	EX1*b*
	0.21×10^{-4}		0.42×10^{-5}	EX1*a*	EX2
	0.15×10^{-4}		0.29×10^{-4}	EX1*a*	EX3
	0.45×10^{-5}		0.23×10^{-4}	EX1*a*	EX4
	0.24×10^{-3}		0.11×10^{-4}	EX1*b*	EX2
	0.12×10^{-4}		0.77×10^{-4}	EX1*b*	EX3
	0.20×10^{-5}		0.19×10^{-4}	EX1*b*	EX4
	0.10×10^{-2}		0.13×10^{-2}	EX2	EX3
	0.24×10^{-5}		0.12×10^{-5}	EX2	EX4
	0.20×10^{-2}		0.18×10^{-2}	EX3	EX4

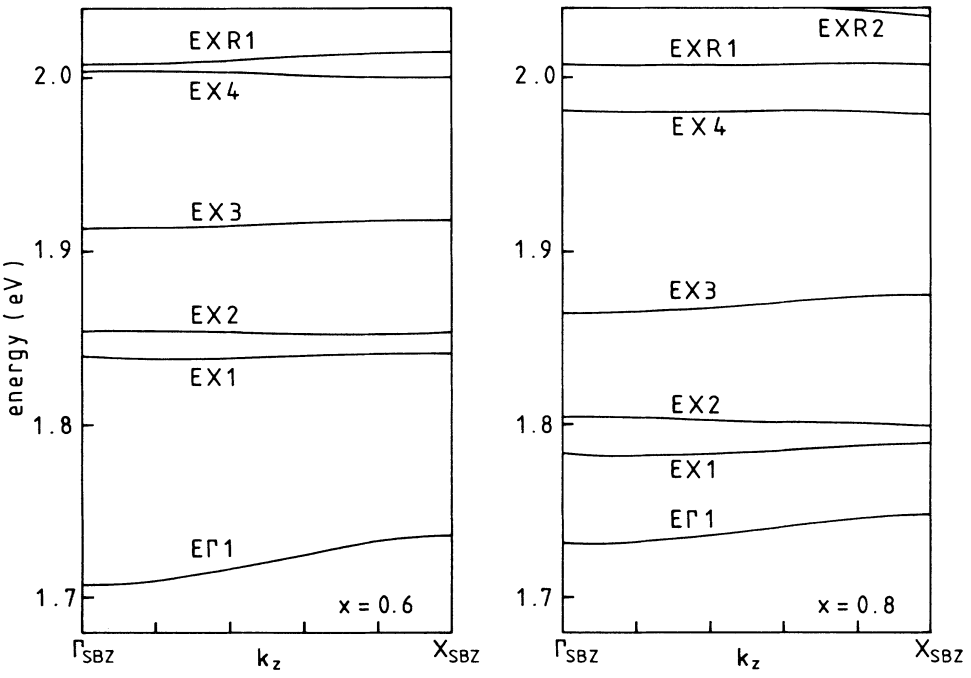

FIG. 7. Dispersions along the Δ_z line between Γ_{SBZ} and X_{SBZ} of the lowest conduction states in the GaAs(28.3 Å)/$Al_xGa_{1-x}As$(28.3 Å) (001) superlattice with $x=0.6$ and $x=0.8$.

TABLE VII. Energies calculated for the zone-center-related states in the GaAs(28.3 Å)/$Al_xGa_{1-x}As$(28.3 Å) (001) superlattice using the pseudopotential method (PP) and Kronig-Penney—type (KP) models (see Table II).

Aluminum fraction x	Method	EΓ1 energy at Γ_{SBZ} (meV)	EΓ1 energy at X_{SBZ} (meV)	EΓR1 energy at X_{SBZ} (meV)
0.2	PP	84	170	277
	KP($+np$)	82	164	279
	KP($-np$)	83	175	296
	KP1($+np$)	89	173	279
	KP1($-np$)	90	187	295
0.6	PP	184	213	
	KP($+np$)	169	192	514
	KP($-np$)	173	201	540
	KP1($+np$)	204	227	536
	KP1($-np$)	220	251	576
0.8	PP	208	225	
	KP($+np$)	190	201	610
	KP($-np$)	195	209	645
	KP1($+np$)	241	252	653
	KP1($-np$)	267	282	726

Å)/$Al_xGa_{1-x}As$(28.3 Å) (001) superlattice with $x=0.6$ and $x=0.8$. In this superlattice, the layers are not thick enough to allow the formation of a DQD amongst the lowest zone-edge-related states and so state EX1 (and the resonant state EXR1) consists of just one state (cf. Figs. 2 and 3). In Table VII, we show energies calculated for the zone-center-related states in the superlattice with $x=0.2$, 0.6, and 0.8 and in Table VIII we show energies calculated for the zone-edge-related states in the superlattice with $x=0.6$. From Table VII it can be seen that, for this superlattice, the best agreement between the pseudopotential and Kronig-Penney results is obtained using the KP1($+np$) prescription. The results in Table VIII show that the effective-mass model gives reasonable results for the zone-edge-related states and, in particular, reproduces state EX1 as a *single* state.

GaAs(50.9 Å)/AlAs(5.7 Å) (001) SUPERLATTICE

In Fig. 8, we show dispersions along the Δ_z line of the SBZ of the lowest conduction states in the GaAs(50.9 Å)/AlAs(5.7 Å) (001) superlattice and in Tables IX and X we show energies calculated for the zone-center- and zone-edge-related states. It can be seen from Table IX that although the barrier (AlAs) region to the zone-center-related states is only one lattice constant in thickness, the Kronig-Penney model with prescription KP($+np$) reproduces very reasonable results. In contrast, however, the effective-mass model is incapable of reproducing the single state EX1 (see Table X), although the energies of the resonant zone-edge-related states in the thicker GaAs layers are well reproduced. These results and conclusions may be compared with those of Schulman and Chang, bearing in mind the different band offsets which were used in the early tight-binding calculations.[18] The effective-mass model should be used with caution for zone-edge-related states in layers consisting of only one or two monolayers.

GaAs(50.9 Å)/$Al_xGa_{1-x}As$(101.8 Å) (001) SUPERLATTICE

We turn our attention to a superlattice with wider GaAs and $Al_xGa_{1-x}As$ layers; some aspects of quantum-well and superlattice structures of similar thickness have been studied elsewhere.[19–22] In Table XI, we compare en-

TABLE VIII. Energies in meV calculated for the zone-edge-related states in the GaAs(28.3 Å)/$Al_{0.6}Ga_{0.4}As$(28.3 Å) (001) superlattice using the pseudopotential method (PP) and Kronig-Penney—type (KP) models (see Table II). Note that state EX1 and EXR1 are *single* states owing to the thickness of the layers. The results indicated with an asterisk have been obtained using an infinite-square-well model combined with the pseudopotential band structure.

	Superlattice state				
method	EX1	EX2	EX3	EX4	EXR1
PP	3—6	18.7—17.5	77.7—83.7	167.5—163.2	172.2—178.6
KP	0.6(*)	30—30	89—89	139—139	170—175
KP1	0.6(*)	22—22	95—95	164—169	170—190

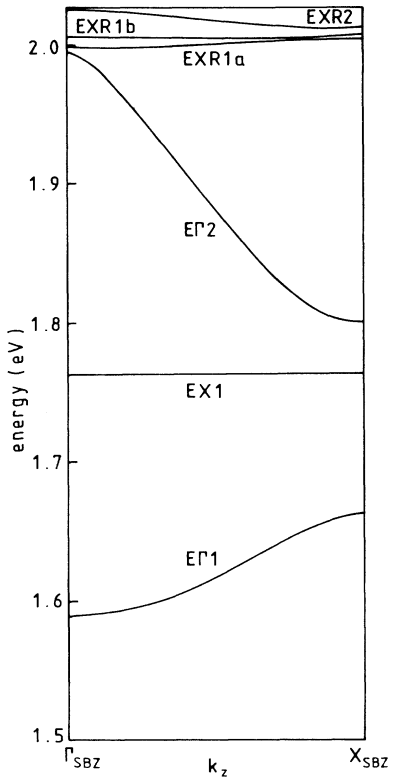

FIG. 8. Dispersions along the Δ_z line between Γ_{SBZ} and X_{SBZ} of the lowest conduction states in the GaAs(50.9 Å)/AlAs(5.7 Å) (001) superlattice. The reader is referred to Ref. 10 where the response of this superlattice to hydrostatic pressure has been discussed in detail.

ergy levels of the lowest zone-edge-related states in the GaAs(50.9 Å)/AlAs(101.8 Å) (001) superlattice obtained using the pseudopotential method with those obtained using an infinite square-well model combined with the pseudopotential band structure. In the infinite square-well model, energies of the superlattice states have been calculated using the polynomial (see Table I) for the zone-edge region of the lowest conduction band of AlAs at wave vectors $k_n = n\pi/L_B$ ($n = 1,2,\ldots$; $L_B = 101.8$ Å) measured from the X point. This simple model appears to

TABLE IX. Energies calculated for the zone-center-related states in the GaAs(50.9 Å)/AlAs(5.7 Å) (001) superlattice using the pseudopotential (PP) method and Kronig-Penney–type (KP) models (see Table II).

Method	EΓ1 energy at Γ_{SBZ} (meV)	EΓ1 energy at X_{SBZ} (meV)	EΓ2 energy at Γ_{SBZ} (meV)	EΓ2 energy at X_{SBZ} (meV)
PP	66	140	278	472
KP($+np$)	67	136	282	476
KP($-np$)	68	145	303	579
KP1($+np$)	92	146	326	495
KP1($-np$)	96	158	375	631

TABLE X. Energies in meV calculated for the zone-edge-related states in the GaAs(50.9 Å)/AlAs(5.7 Å) (001) superlattice using the pseudopotential (PP) method and Kronig-Penney–type (KP) models (see Table II). The KP models fail to reproduce state EX1.

		Superlattice state		
Method	EX1	EXR1a	EXR1b	EXR2
PP	26	260–266	268–268	274–287
KP		255–255	276–276	281–282
KP1		253–253	275.2–275.9	278.7–281.7

reproduce well the energies of the lowest (best-confined) zone-edge-related states even though the Δ_5 minima are regions where the bulk states vary rapidly with $\mathbf{k}$ and for which an effective-mass description is difficult to justify. In the camel's-back region, the effective mass is high and the tunneling amplitude of the states, in the absence of Γ-X mixing, is effectively zero. In Table XII, we compare energy levels for the lowest zone-center-related states in the GaAs(50.9 Å)/$Al_{0.3}Ga_{0.7}As$(101.8 Å) (001) superlattice obtained using the pseudopotential method and Kronig-Penney–type models. We note, in particular, that the effective-mass model is capable of reproducing well the resonant zone-center-related states which are confined predominantly in the alloy layers and which have energies in the hot-electron region.

SUMMARY

We have shown the form of the subband dispersions associated with superlattice conduction states derived from the principal and the secondary minima in several GaAs-$Al_xGa_{1-x}As$ (001) superlattices. In particular, dispersions of interacting zone-center- and zone-edge-related states have been shown and the zone-folding effect has

TABLE XI. Energies calculated for the lowest zone-edge-related states in the GaAs(50.9 Å)/(AlAs(101.8 Å) (001) superlattice. On the left-hand side are energies obtained from the pseudopotential calculation and on the right-hand side are energies E_n calculated from the polynomial fit to the band structure of AlAs (see Table I) at wave vectors $k_n = n\pi/L_B$ ($n = 1,2,\ldots$; $L_B = 101.8$ Å) measured from the X point.

	Pseudopotential calculation	Infinite square-well model	
State	Energy (meV)	Quantum number n	Band-structure energy, E_n (meV)
EX1a	0.4	3	0.1
EX1b	1.2	2	1.3
EX2a	2.4	4	3.2
EX2b	6.7	1	5.5
EX3	9.2	5	12.1
EX4	18.8	6	27.2
EX5	36.8	7	49.1
EX6	57.8	8	78.0
EX7	88.8	9	114.0

TABLE XII. Energies calculated for the zone-center-related states in the GaAs(50.9 Å)/$Al_{0.3}Ga_{0.7}As$(101.8 Å) (001) superlattice using the pseudopotential (PP) method and Kronig-Penney–type (KP) models (see Table II).

Method	EΓ1 energy at Γ_{SBZ} (meV)	EΓ1 energy at X_{SBZ} (meV)	EΓ2 energy at Γ_{SBZ} (meV)	EΓ2 energy at X_{SBZ} (meV)	EΓR1 energy at Γ_{SBZ} (meV)	EΓR1 energy at X_{SBZ} (meV)
PP	82.4	82.7	256.9	264.6	312.5	342.4
KP($+np$)	70.3	70.4	236	240	311	337
KP($-np$)	71.5	71.6	244	251	315	350
KP1($+np$)	80.8	80.8	250	255	311	341
KP1($-np$)	83.5	83.5	261	272	315	359

been demonstrated. We have shown that the zone-center–zone-edge mixing manifests itself in an intricate weaving of zone-center charge-density components through the charge densities of the zone-edge-related states. Along the superlattice axis, the zone-center charge density twists between each peak in the charge-density "envelopes" of the zone-edge-related states. This twisting is linked to the atomic layout within each layer and is the mechanism by which (mixed) zone-center- and zone-edge-related states are orthogonalized. Detailed comparisons between results of the pseudopotential calculations and results obtained using Kronig-Penney–type analyses have been made. Although no particular prescription for effective masses was found to consistently work best, the results obtained from the effective-mass model were generally in reasonable agreement with the pseudopotential results. The results do indicate, however, that for zone-center-related states the averaging prescription (i.e., KP model; see Table II) works best for superlattices with ultrathin barriers where the subband dispersion is appreciable, but starts to break down for thicker barriers. The KP1 prescription is the commonly used one and it is not surprising that there is good agreement with the pseudopotential results for superlattices with wide wells and wide barriers. However, it is unusual that the KP rather than the KP1 prescription works best for the ultrathin case, although it is equally important to bear in mind that such models appear to work well *even* for cases in which the superlattices layers are only a few Å in width. We suspect that the explanation of this result is connected with a self-consistent process of energy difference minimization which tends to produce a band-structure configuration of maximum wave function "smoothness"; the actions of such a process are especially important close to the band edges. We believe that this one-to-one global, i.e., entire bulk Brillouin zone, minimization of phase differences between (GaAs and $Al_xGa_{1-x}As$) Bloch functions is an important mechanism in the determination of band offsets and the formation of the spectrum of confined states and may explain the success of effective-mass-type models even for ultrathin layers. This is the subject of a forthcoming paper.[23] The importance of such phase differences has already been demonstrated in connection with the processes of confinement[9,24] and the control of Γ-X mixing.[10]

We suggest that the modified effective-mass Hamiltonian model presented above—in which information about the phases of the zone-center- and zone-edge-related states is incorporated to take account of interference effects associated with intervalley scattering—should provide a useful basis for studying hot-electron transport properties of superlattices and for device modeling. Anticrossing behavior, both of energy levels and optical matrix elements, can be handled readily within perturbation theory.

*Present address: British Telecom Research Laboratories, Martlesham Heath, Ipswich, Suffolk, IP5 7RE, United Kingdom.

[1]M. A. Gell, D. Ninno, M. Jaros, and D. C. Herbert, Phys. Rev. B **34**, 2416 (1986).
[2]M. Jaros, K. B. Wong, and M. A. Gell, Phys. Rev. B **31**, 1205 (1985).
[3]M. A. Gell, Ph.D. thesis, University of Newcastle upon Tyne, 1986.
[4]A. A. Kopylov, Solid State Commun. **56**, 1 (1985).
[5]D. Mukherji and B. R. Nag, Phys. Rev. B **12**, 4338 (1975).
[6]J. P. Vigneron and Ph. Lambin, J. Phys. A **12**, 1961 (1979).
[7]J. P. Vigneron and Ph. Lambin, J. Phys. A **13**, 1135 (1980).
[8]E. M. Conwell and M. O. Vassel, Phys. Rev. **166**, 797 (1968).
[9]M. A. Gell, K. B. Wong, D. Ninno, and M. Jaros, J. Phys. C **19**, 3821 (1986).
[10]M. A. Gell, D. Ninno, M. Jaros, D. J. Wolford, T. F. Keuch, and J. A. Bradley, Phys. Rev. B **35**, 1196 (1987).
[11]S. L. Richardson, M. L. Cohen, S. G. Louie, and J. R. Chelikovsky, Phys. Rev. B **33**, 1177 (1986).
[12]G. B. Bachelet and N. E. Christensen, Phys. Rev. B **31**, 879 (1985).
[13]D. J. Wolford, T. F. Keuch, J. A. Bradley, M. A. Gell, D. Ninno, and M. Jaros, J. Vac. Sci. Technol. **B4**, 1043 (1986).
[14]A. I. Gubanov and F. M. Gashimzade, Fiz. Tverd. Tela. **1**, 1411 (1959) [Sov. Phys.—Solid State **1**, 1294 (1960)], and references therein.
[15]C. J. Bradley and A. P. Cracknell, *Mathematical Theory of Symmetry in Solids* (Clarendon, Oxford, 1972).
[16]D. Ninno (private communication).
[17]L. C. West and S. J. Eglash, Appl. Phys. Lett. **46**, 1156 (1985).

[18]J. N. Schulman and Y. C. Chang, Phys. Rev. B **24**, 4445 (1981).
[19]A. C. Marsh and J. C. Inkson, IEEE J. Quantum Electron. **22**, 58 (1986).
[20]E. E. Mendez, E. Calleja, C. E. T. Goncalves da Silva, L. L. Chang, and W. I. Wang, Phys. Rev. B **33**, 7368 (1986).
[21]T. J. Drummond and I. J. Fritz, Appl. Phys. Lett. **47**, 284 (1985).
[22]J. N. Schulman and Y. C. Chang, Phys. Rev. B **31**, 2056 (1986).
[23]M. A. Gell and D. C. Herbert (unpublished).
[24]M. Jaros, K. B. Wong, M. A. Gell, and D. J. Wolford, J. Vac. Sci. Technol. **B3**, 1051 (1985).